Systematic shifts in Budyko relationships caused by groundwater storage changes

Laura E. Condon[1*] and Reed M. Maxwell[2]

[1]Department of Civil and Environmental Engineering, Syracuse University, Syracuse, NY USA

[2]Integrated GroundWater Modeling Center, Department of Geology and Geological Engineering, Colorado School of Mines, Golden CO USA

**Correspondence to: lecondon@syr.edu*

Abstract:

Traditional Budyko analysis is predicated on the assumption that the watershed of interest is in dynamic equilibrium over the period of study and thus surface water partitioning will not be influenced by changes in storage. However, previous work has demonstrated that groundwater surface water interactions will shift Buydko relationships. While Budyko approaches have been proposed to account for storage changes, given the limited ability to quantify groundwater fluxes and quantity across spatial scales, additional research is needed to understand the implications of these approximations. This study evaluates the impact of storage changes on Budyko relationships given three common approaches to estimating evapotranspiration fractions: (1) determining evapotranspiration from observations, (2) calculating evapotranspiration from precipitation and surface water outflow, (3) adjusting precipitation to account for storage changes. We show conceptually that groundwater storage changes will shift Budyko relationship differently depending on the way evapotranspiration is estimated. A one-year transient simulation is used to mimic all three approaches within a numerical framework in which groundwater surface water exchanges are prevalent and can be fully quantified. The model domain spans the majority of the Continental US and encompasses 25,000 nested watersheds ranging in size from 100 km^2 to over 3,000,000 km^2. Model results illustrate that storage changes can generate different spatial patterns in Budyko relationships depending on the approach used. This shows the potential for systematic bias when comparing studies

that use different approaches to estimate evapotranspiration. Comparisons between watersheds are also relevant for studies that seek to characterize variability in the Budyko space using other watershed characteristics. Our results demonstrate that within large complex domains the correlation between storage changes and other relevant watershed properties, such as aridity makes it difficult to easily isolate storage changes as an independent predictor of behavior. However, we suggest that using the conceptual models presented here comparative studies could still easily evaluate a range of spatially heterogeneous storage changes by perturbing individual points to better incorporate uncertainty in storage changes into analysis.

1. Introduction:

The Budyko hypothesis states that the fraction of precipitation (P) that leaves a watershed through evapotranspiration (E), as opposed to runoff, can be predicted by the aridity of the watershed [*Budyko*, 1958; 1974]. *Budyko* [1974] compared long-term evapotranspiration fractions to aridity for 1,200 large watersheds around the globe and showed that 90% of the variance in evapotranspiration ratio (E/P) could be described by a single empirical curvilinear equation dependent only on aridity, often referred to as the "Budyko Curve". Budyko noted that this consistent relationship is a reflection of the dominance of macroclimate over large drainage areas and long time periods where it can be assumed that a watershed is in steady state (i.e. when it can be assumed that there are no storage changes over the period of analysis).

The simplicity of this relationship has since garnered much interest within the hydrologic community for its potential to predict watershed behavior using only climate variables, which are often easier to observe than many hydrologic variables, and without relying on computationally expensive or heavily parameterized numerical models. In recent years, the Budyko hypothesis has also been put forward as a way of predicting hydrologic sensitivity to climate change especially in ungauged basins [e.g. *Donohue et al.*, 2011; *Jones et al.*, 2012; *Renner et al.*, 2014]. However, application of

this method has been partially limited by spatial variability between watersheds and the required steady state assumption.

The original Budyko curve presented a universal relationship between evapotranspiration and aridity [*Budyko*, 1974]. Subsequent work has shown that, while the Budkyo curve is generally robust, climate alone is not sufficient to predict watershed partitioning; the shape of the curve can vary between locations, especially for smaller watersheds. Differences in behavior between river basins have been attributed to seasonal lags in water and energy supply, vegetative and soil properties [*Donohue et al.*, 2007]. The original Budyko curve has been reformulated multiple times to incorporate additional free parameters to reflect these differences [*Choudhury*, 1999; *Fu*, 1981; *Milly*, 1994; *L. Zhang et al.*, 2001; *L. Zhang et al.*, 2004], and numerous studies have used these modified formulations to relate curve parameters to physical basin characteristics in many settings [e.g. *Li et al.*, 2013; *Shao et al.*, 2012; *Williams et al.*, 2012; *Xu et al.*, 2013; *Yang et al.*, 2009]. For example, *Li et al.* [2013] and *Yang et al.* [2009] evaluated relationships between the shape of the Budyko curve and vegetation coverage. Similarly, *Williams et al.* [2012] and *L. Zhang et al.* [2004] found distinct shape parameters when comparing forested watersheds to grasslands, although it should be noted that they reached the opposite conclusion about their relative magnitudes. Others have focused on the role of soil moisture and noted differences in behavior based on plant water availability and seasonal lags in supply and demand [e.g. *Milly*, 1994; *Yang et al.*, 2007; *Yokoo et al.*, 2008].

Many previous studies have demonstrated good predictive abilities using modified Budyko formulations even when applied to smaller watersheds and shorter time scales than those originally intended. However, poor performance in some locations, especially over annual or seasonal time periods, has been attributed to the influence of storage changes that violate the steady state assumption [*Milly and Dunne*, 2002; *Lu Zhang et al.*, 2008]. *Istanbulluoglu et al.* [2012] and *T Wang et al.* [2009] showed interannual storage changes can produce a negative correlation between evapotranspiration ratio and aridity that is counter to the Budyko curve for baseflow

dominated basins in the Nebraska Sand Hills. *D Wang* [2012] evaluated inter-annual storage changes for twelve watersheds in Illinois and showed that, on an annual timescale, variability in runoff and storage is larger than evapotranspiration, and accounting for storage can improve the performance of Budyko predictions. *Du et al.* [2016] presented a method for explicitly accounting for storage changes within the Budyko framework and demonstrated that this approach can greatly improve performance in arid regions or over shorter time scales where the steady state assumption is not valid.

These studies all indicate the potential importance of groundwater surface water interactions within the Budyko framework and illustrate paths forward for incorporating groundwater surface water interactions into Budyko analysis. However, the extensive field work needed to fully quantify groundwater surface water exchanges is often not possible and is counter to the simplicity and minimal data requirements of the Budyko approach. Even in Budyko analysis focused on groundwater surface water interactions, quantifying groundwater changes remains a limiting factor. For example, in some studies, the impact of groundwater storage changes have been inferred from variability around the Budyko relationship without directly measuring these changes [*Milly and Dunne*, 2002; *Lu Zhang et al.*, 2008]. Others have addressed interactions more directly using baseflow separation techniques that require only streamflow observations [*T Wang et al.*, 2009] or lumped watershed models that parameterize baseflow and recharge [*Du et al.*, 2016]. However, with both of these approaches the groundwater system is still not directly simulated or observed. *Istanbulluoglu et al.* [2012] and *D Wang* [2012] did use observations of water table depth to directly quantify storage changes and demonstrate the impact of this change within the Budyko framework; but the study areas with this approach were relatively limited (four watersheds for *Istanbulluoglu et al.* [2012], and twelve for *D Wang* [2012]). Groundwater observations sufficient to precisely characterize watershed storage changes are difficult to obtain and are not widely available. Therefore, adding groundwater storage calculations into

Budyko analyses remains infeasible in many cases and more work is needed to understand the sensitivity of Budyko relationships to changes in storage

There are three common approaches to estimate evapotranspiration (E) in Budyko analysis (listed here in order of complexity): First, if E can't be measured directly, it is often estimated as the difference between precipitation and river outflow in a basin. Second, E can be measured directly using a variety of field methods. Third, as is the case with the more recent studies that seek to account for storage changes, observed E values can be augmented with measurements of groundwater surface water exchanges to estimate the 'effective precipitation' that is available for surface processes (i.e. outflow and E). Here we hypothesize that storage changes will bias Budyko results in predictable ways, as has been indicated by previous studies, but that the direction of the bias will vary based on the way that evapotranspiration is handled within a study. We evaluate this hypothesis by comparing Budyko relationships generated following the three different approaches using the outputs of a physically based hydrologic model that directly simulates the integrated groundwater surface water system over a large spatial domain at high resolution. The three primary goals of our comparative analysis are as follows:

- 1. Evaluate the sensitivity of Budyko relationships to groundwater storage changes
- 2. Characterize systematic differences in the impact of storage changes on Budyko relationships
- 3. Illustrate variability between approaches across physical settings and spatial scales

2. Methods

We use an integrated hydrologic model to simulate water and energy fluxes in both the surface and the subsurface. Here we apply a high resolution (1 km^2) simulation of the majority of the continental U.S. which covers more than 6 M km^2 and simulates hydrologic systems across a broad range of physical settings and storage change magnitudes. The model is driven using historical observed atmospheric forcings such as

precipitation and temperature and provides gridded outputs of all water and energy fluxes throughout the system. We use simulated surface water flow, evapotranspiration and groundwater surface water exchanges to calculate Budyko relationships using three different approaches to estimate fluxes:

1. Calculating evapotranspiration from simulated runoff and precipitation
2. Using simulated evapotranspiration values directly
3. Using simulated evapotranspiration values directly and taking into account storage changes.

Differences between the approaches are compared with storage changes in each basin to evaluate the systematic impacts of these changes on Budyko relationships.

The numerical modeling approach used here provides several important advantages for this type of analysis. Within the model, groundwater surface water exchanges for every watershed in the system are fully characterized. This guarantees perfect closure of the water balance and means that we can mimic all three approaches within a consistent numerical framework where storage changes are directly accounted for. Furthermore, because the goal is to understand differences between approaches and not to predict local Budyko parameters the key advantage here is the ability to evaluate physically realistic behavior across a variety of physical settings and spatial scales where groundwater can be fully accounted for. Within this context, it should also be noted that the focus is on how groundwater storage changes perturb relationships. Therefore, uncertainty in local model parameters is much less important than realistic simulation of physical interactions for a range of storage changes and aridity values within a controlled numerical framework.

Sections 2.1 and 2.2 detail the numerical modeling approach and the continental scale simulation used for analysis. An explanation of the source of each of the relevant water balance terms generated from the model is provided in Section 2.3. Sections 2.4 and 2.5 explain the three different approaches for ET estimation and how they are evaluated within the Budyko Framework.

175 **2.1 Hydrologic Modeling**

176 Previous work has evaluated the Budyko curve using hydrologic models of varying levels
177 of complexity. The abcd model employed by *Du et al.* [2016], among others, is a lumped
178 water balance model that includes baseflow and groundwater recharge using calibrated
179 parameters. *Yokoo et al.* [2008] used a different water balance model with a more
180 complex groundwater formulation that includes saturated and unsaturated zones, but
181 the authors noted limitations in simulating infiltration excess overland flow with this
182 approach. *Gentine et al.* [2012] applied a water balance model that includes a soil
183 bucket and can simulate infiltration excess overland flow; however it did not include
184 topography and was only applied at the plot scale. While these approaches do account
185 for storage in the subsurface and varying levels of complexity in groundwater surface
186 water exchanges, they all take a lumped approach and rely on calibrated parameters
187 that are not physically based. The lumped parameter approach is illustrated in Fig. 1a.

188 Increasing in sophistication, *Troch et al.* [2013] used a semi-distributed model
189 that included shallow perched aquifers as well as root zone and soil moisture dynamics;
190 and *Koster and Suarez* [1999] evaluated a global circulation model that simulated land
191 surface and atmospheric processes using physically based equations. Incorporating
192 more sophisticated physical processes increases computational expense especially for
193 large high-resolution domains. To address this, *Koster and Suarez* [1999] used a global
194 simulation but at low spatial resolution (4° by 5°), while *Troch et al.* [2013] limited their
195 analysis to the hillslope scale. Furthermore, both of these approaches are focused on
196 the land surface and shallow subsurface and neither included lateral groundwater flow
197 as shown in Fig. 1b.

198 To the authors' knowledge, no one has evaluated Budyko behavior over large
199 spatial scales using a hydrologic model that integrates lateral groundwater flow with
200 surface processes (Fig. 1c). So called integrated hydrologic models that incorporate
201 physically based lateral groundwater flow with overland flow and land surface processes
202 are a relatively new development in hydrologic modeling. These tools are ideal for
203 capturing dynamic behavior and interactions throughout the terrestrial hydrologic cycle

and they have been increasingly applied over the last decade. To achieve this level of complexity requires significant computational resources, and detailed model inputs. These requirements have generally limited the application of integrated tools to regional scale domains. Continental-scale high-resolution simulations have only recently become technically feasible.

For this analysis, we use the first high-resolution integrated groundwater surface water simulation of the majority of the continental US (CONUS) [*Maxwell and Condon*, 2016; *Maxwell et al.*, 2015]. The CONUS simulation was developed using the integrated hydrologic model ParFlow-CLM [*Kollet and Maxwell*, 2006; 2008; *Maxwell and Miller*, 2005]. ParFlow simulates three-dimensional variably saturated groundwater flow using Richards' equation:

$$S_s S(\psi_p) \frac{\delta \psi_p}{\delta t} + \phi \frac{\delta S(\psi_p)}{\delta t} = \nabla \cdot \left[-K_s(x) k_r(\psi_p) \cdot \nabla(\psi_p - z) \right] + q_s \quad (1)$$

where S_s is the specific storage [L^{-1}], S is the relative permeability [-], which varies with pressure head ψ_p [L] based on the *Van Genuchten* [1980] relationships, t is time [T], ϕ is the porosity of the subsurface [-], $K_s(x)$ is the saturated hydraulic conductivity tensor [LT^{-1}], K_r is the relative permeability [-], which also varies with pressure head according to the *Van Genuchten* [1980] relationships, z is the depth below the surface [L] and q_s is a source/sink term [T^{-1}]. Note that units of T^{-1} for the flux terms reflects the fact that they are scaled by the cell thickness.

Overland flow is included in the groundwater flux term of Eq. (1) (i.e. in the first term on the right hand side) using a free surface overland flow boundary condition that applies continuity of pressure and flux across the boundary between the land surface and the subsurface. Overland flow is solved using the kinematic wave approximation of the momentum equation where the diffusion terms are neglected and it is assumed that the bed slope, S_o [-] is equivalent to the friction slope. Flow varies as a function of ponded depth according to Manning's equation:

$$v = \frac{\sqrt{S_o}}{n} \psi_p^{2/3} \quad (2)$$

where n [$TL^{-1/3}$] is the Manning's roughness coefficient. Using this approach ParFlow is able to solve variably saturated groundwater flow and overland flow simultaneously. Practically this means that (1) the location of surface water bodies do not need to be specified a priori and will develop wherever water ponds in the domain, and (2) two-way groundwater surface water exchanges can evolve dynamically based on head gradients and subsurface properties.

ParFlow is also coupled with a land surface model derived from the Common Land Model (CLM) [*Dai et al.*, 2003]. In the combined ParFlow-CLM model [*Kollet and Maxwell*, 2008], ParFlow solves the water balance in the subsurface and CLM solves the combined water energy balance at the land surface. At the land surface, the energy balance (R_{net}) is comprised of sensible (H), latent (LE) and Ground (G) heat fluxes [Wm^{-2}]:

$$R_{net} = H + LE + G \quad (3)$$

All of the energy fluxes listed in Eq. (3) vary with soil moisture. CLM uses pressure head and saturation values for the upper subsurface layers (in this case the top 2m) simulated by ParFlow and passes infiltration fluxes back to ParFlow. Land surface processes are also driven by atmospheric forcing variables, which are provided as inputs to the model. Forcing variables include short and longwave radiation, precipitation, air temperature, atmospheric pressure, specific humidity and wind. Using these inputs, CLM simulates multiple land surface processes including canopy interception, evaporation from the canopy and the ground surface, plant transpiration, ground and sensible heat fluxes as well as snow dynamics.

This study focuses on simulated evapotranspiration E [LT^{-1}], which is the sum of evaporation Ev, and plant transpiration T. CLM uses a mass transfer approach with mean variables where evaporation is calculated using the gradient between the specific humidity at the ground surface, q_g [MM^{-1}], and the specific humidity at a reference

height, q_a [MM^{-1}], scaled by a soil resistance factor β [-], air density ρ_a and the atmospheric resistance, r_d [-] as follows:

$$Ev = -\beta \rho_a \frac{q_g - q_a}{r_d} \quad (4)$$

The soil resistance factor is calculated based on the saturation relative to the residual saturation and the saturation in the uppermost soil column (refer to *Jefferson and Maxwell* [2015] for the complete formulation).

Similarly transpiration is calculated by scaling the potential evapotranspiration to account for stomatal and aerodynamic resistance as follows

$$T = \left(R_{pp,dry} + L_w\right) L_{SAI} \left(\rho_a \frac{q_{sat} - q_a}{r_d}\right) \quad (5)$$

Here $R_{pp,dry}$ [-] is a scaling parameter, L_w [-]is the fraction of the canopy that is covered in water, L_{SAI} is leaf and stem area index and q_{sat} [-] is the saturated specific humidity [mm-1]. $R_{pp,dry}$ is a function of light and moisture limitations. Parameters that are used to determine leaf area index, reflectance and transmittance and root distributions vary by land cover type and are provided as inputs to the model using the 18 land cover classes defined by the International Geosphere Biosphere Program (IGBP). For additional details on the numerical approach and analysis on the sensitivity of evaporation and transpiration within CLM the reader is referred to [*Ferguson et al.*, 2016; *Jefferson and Maxwell*, 2015; *Kollet and Maxwell*, 2008; *Maxwell and Condon*, 2016].

2.2 Model domain and simulations

The analysis presented here is based on a previously developed transient ParFlow-CLM simulation of the majority of the Continental US (CONUS) documented in *Maxwell and Condon* [2016]. The CONUS domain covers the majority of eight major river basins, shown in Fig. 2 and spans roughly 6.3M square kilometers at 1km lateral resolution. The integrated physically based approach employed for this simulation requires significant

290 computational resources. However, there are several key benefits that warrant this
291 costly approach; this simulation (1) provides high-resolution (1 km^2) gridded outputs
292 that fully define water and energy fluxes from the groundwater through the land surface
293 without calibration, (2) requires a minimal number of empirical parameters and (3)
294 directly simulates variably saturated lateral groundwater flow which has not been
295 incorporated in previous models used for Budyko analysis.
296 As detailed in in *Maxwell and Condon* [2016] and *Maxwell et al.* [2015], the
297 model extends 102 m below the subsurface with five vertical layers that contour to the
298 land surface using a terrain following grid formulation [*Maxwell*, 2013]. The vertical
299 resolution of the domain decreases with depth to better resolve the shallow subsurface.
300 Layer thicknesses are 0.1, 0.3, 0.6, 1 and 100m moving from the land surface down.
301 Spatially heterogeneous physical parameters for the subsurface include porosity,
302 saturated hydraulic conductivity and van Genuchten parameters. Subsurface spatial
303 units were determined using a national permeability map developed by *Gleeson et al.*
304 [2011] for the bottom 100 m of the domain and the soil survey geographic database
305 (SSURGO) for the top two meters. Maps of the subsurface units and their properties are
306 available in *Maxwell and Condon* [2016] and *Maxwell et al.* [2015]. The land surface was
307 derived from the Hydrologic data and maps based on the Shuttle Elevation Derivatives
308 at multiple Scales (HydroSHEDS) digital elevation model using a topographic processing
309 algorithm to ensure fully connected drainage network [*Barnes et al.*, 2016]. Vegetation
310 types were extracted from the USGS land cover dataset using the IGBP land cover
311 classifications.
312 The model was first initialized to a steady state groundwater configuration using
313 the ParFlow model without CLM starting from a completely dry domain and providing a
314 constant recharge forcing over the land surface to achieve a dynamic equilibrium.
315 Development of this steady state simulation and evaluation of the resulting
316 groundwater configuration are provided in [*Condon et al.*, 2015; *Maxwell et al.*, 2015].
317 Using the steady state groundwater configuration as a starting point, and following
318 some initialization period, the coupled ParFlow-CLM model was used to simulate the

319 fully transient system including land surface processes for water year 1985 (i.e. Oct. 1,
320 1984 through Sep., 30 1985), which was chosen as it is the most climatologically average
321 within the past 30 years. The transient simulation was driven by historical hourly
322 meteorological forcings for water year 1985 from the North American Land Data
323 Assimilation System Phase 2 (NLDAS 2) [*Cosgrove et al.*, 2003; *Mitchell et al.*, 2004].
324 Anthropogenic activities such as groundwater pumping and surface water storage are
325 not included in the transient simulation. Therefore the simulation represents natural
326 flows in a pre-development scenario, which is ideal for Budyko analysis. Complete
327 details of the development of the transient simulation are available in *Maxwell and*
328 *Condon* [2016].

329 The one-year simulation presented here intentionally violates the steady state
330 assumption. The purpose of our analysis is to evaluate the impact of net storage
331 changes on Budyko relationships, therefore a steady-state simulation is not the goal. It
332 can also be argued that storage changes will vary from year to year or depending on the
333 multi-year period analyzed. The 1985 simulation year is not presented as a prediction of
334 long-term storage variability, it is simply used to sample a range of groundwater surface
335 water exchange across variable climates and physical settings. We present a general
336 framework for understanding the impacts of storage changes in various Buydko
337 formulations using water year 1985 as a representative example.

338 Similarly, because we are focused on a comparative analysis within the Budyko
339 framework, the results are not dependent on local calibration between simulated
340 results and observations. The discrepancies between approaches stem from differences
341 in the variables used to create a water balance (refer to sections 2.3 and 2.4); these
342 findings are not sensitive to parameter uncertainty in the model. Still, the transient
343 simulation has been rigorously validated against all publically available observations for
344 water year 1985. This includes transient observations at varying frequencies from 3,050
345 stream gauges, 29,385 groundwater wells and 378 snow stations for a total of roughly
346 1.2 million comparisons points. Flux tower observations were not available over this
347 period, but latent heat fluxes were also compared to the Modern Era Retrospective-

analysis for Research and Application (MERRA) dataset. Complete details of the model validation are provided in the supplemental information of *Maxwell and Condon* [2016].

Although there are of course limitations to the model and significant uncertainties in spatial model parameterization, especially for the subsurface, overall comparisons between simulated and observed values demonstrate that the modeling approach is robust. Stream-flow timing and magnitude are generally well matched in undeveloped basins, snowpack timing and melt is accurate and spatial patterns in latent heat flux are reasonable. Most importantly for this analysis, the model validation shows that ParFlow is accurately capturing the relevant physical processes. Uncertainty in subsurface parameterization, bias in atmospheric forcing data and lack of anthropogenic activities were identified as key areas that could improve the local predictions of the model. However, as discussed above, the purpose of this work is not to predict Budyko curve parameters for water year 1985. The uncertainties listed here are therefore important to note, but do not limit the utility of this tool as a test bed for evaluating interactions across spatial scales and complex physical settings.

2.3 Water Balance Components

Outputs from the hydrologic simulation are used to quantify all of the relevant water balance components for Budyko analysis. Precipitation is an input to the ParFlow CLM model. Within the model precipitation can infiltrate to the subsurface, contribute to runoff or pond on the land surface. Evaporation occurs from ponded water, bare soil and canopy interception. Additionally, roots pull water from the subsurface to support transpiration for plants and lateral groundwater flow redistributes moisture within the subsurface and can further support overland flow. All of these processes occur within every 1 km^2 grid cell in the domain. The focus of this work is on watershed function and therefore the gridded results are aggregated to more hydrologically relevant units. The domain is divided into 33,454 subbasins each containing a single stream. Subbasin areas, outlined in Fig. 2, vary but are generally on the order of 100 km^2. The total drainage area for every subbasin, henceforth referred to as the watershed, is defined by

tracing up the river network to encompass the entire upstream contributing area. This results in 33,454 nested watersheds ranging in drainage area from about one hundred square kilometers to over three million. For all of the following analysis we will focus on the 24,235 watersheds that are contained within the highlighted regions of Fig. 2. Similarly, while the simulation uses an hourly time step, here we evaluate annual values.

At the watershed scale, precipitation P [L^3] is balanced by surface water outflows, Q_{out} [L^3], evapotranspiration, E [L^3], and net groundwater surface water exchanges, referred to as groundwater contributions, G [L^3].

$$P = Q_{out} + E + G \tag{6}$$

Equivalently this can be expressed in terms of ratios relative to incoming precipitation where the sum of the outflow ratios sum to one:

$$1 = \frac{Q_{out}}{P} + \frac{E}{P} + \frac{G}{P} \tag{7}$$

As noted above, every watershed fully encompasses its contributing area, and therefore surface water inflows are zero. P is the sum of the gridded annual precipitation over the drainage area. Every watershed is defined to have a single outlet point. Q_{out} is the overland flow calculated hourly at the outlet using the ponded water depth and Eq. (2) and summed over the simulation period. E is the total evaporation and transpiration simulated by ParFlow-CLM summed for every grid cell in the drainage area over the year.

There are multiple ways to estimate groundwater contributions within the model. Using gridded model outputs, the exchanges across the boundaries of every river cell can be summed to determine net contribution of groundwater to overland flow. Similarly, we can aggregate hourly changes in groundwater storage for every sub basin to determine total storage exchanges. Because we are interested in the net contribution of groundwater to streamflow and evapotranspiration for this analysis, we

406 can take a simpler approach. Within our numeral framework we have guaranteed
407 closure of the water balance for every watershed and therefore the net change in
408 groundwater storage that contributes to the surface water budget is simply $P - Q_{out} - E$
409 based on Eq. (6). When calculated this way G encompasses the total groundwater
410 surface water exchanges (i.e. changes in storage) required to support the simulated
411 outflow and evapotranspiration. It should be noted that in this formulation G
412 encompasses both exchanges between groundwater and surface water, which can be
413 either positive fluxes from the surface to the subsurface or negative fluxes from
414 subsurface to the surface, as well as changes in surface water storage. The assumption is
415 that, over the annual simulation, changes in ponded water are small relative to
416 groundwater surface water exchanges and so we refer to G as simply groundwater
417 storage changes or groundwater contributions. We follow the convention that a positive
418 groundwater contribution denotes water that is infiltrating from the land surface to the
419 subsurface whereas a negative value indicates groundwater discharge which can either
420 occur from groundwater supported *E* or baseflow contributions to streams.
421 This approach is focused solely on the net contribution of groundwater to the
422 surface water budget. Nested systems of local and regional lateral groundwater flow are
423 simulated within the model and previous work has evaluated spatial patterns and
424 physical drivers of lateral groundwater imports and exports across the domain [*Condon*
425 *et al.*, 2015; *Maxwell et al.*, 2015] as well as groundwater residence times [*Maxwell et*
426 *al.*, 2016]. Here we focus only on net exchanges with the surface that are relevant to the
427 Buyko formulation. We do not need to quantify lateral exchanges in the subsurface
428 directly for these purposes; however, it should be noted that the lateral redistribution of
429 groundwater that occurs within the model is still vital to generating realistic
430 groundwater configurations and supporting groundwater surface water exchanges.
431 In addition to the simulated evapotranspiration (*E*), potential evaporation E_p is
432 calculated using Eq. (4), the hourly meteorological forcing data used to drive the
433 simulations (air temperature, atmospheric pressure, specific humidity, and wind speed),
434 and simulated ground temperatures in the uppermost layer of the model. To calculate

potential evaporation, as opposed to E, the β parameter is set to one to eliminate soil resistance and q_g is the saturated specific humidity calculated based on the ground temperature and atmospheric pressure. As with E, hourly gridded E_p values are summed over the entire simulation period for every watershed drainage area. Using the modeled simulated ground temperatures and model inputs to calculate E_p ensures that the E_p values driven by the same water and energy inputs that control E in the simulation.

Fig. 3 maps the aridity index (E_p/P) as well as each component of the water balance from Eq. (7) expressed as ratios of precipitation. Subplots b and c show regional trends in the relative importance of evapotranspiration as opposed to overland flow. In the more arid western portions of the domain (shown in red on subplot a), Q_{out} is small compared to E whereas in the more humid eastern portions of the domain (blue and orange values in subplot a) the relative magnitude of Q_{out} increases.

Within this annual simulation, subplot d shows that groundwater surface water exchanges (G/P) can be a substantial portion of the water balance in much of the domain. This indicates that the system in not in steady state over the simulation period. As discussed in Section 2.2 the one-year simulation time was intentionally selected for this reason. Here, we take advantage of the ability to directly calculate groundwater surface water exchanges within a controlled numerical simulation where such exchanges are prevalent in order to evaluate the impact of storage changes on Buydko relationships across a range of spatial scales and climates.

The groundwater contribution ratio map also illustrates the importance of lateral groundwater flow at multiple spatial scales within the system. Groundwater storage gains (i.e. positive values of G/P) are prevalent in the western arid portion of the domain and groundwater discharge to surface water is more common in the humid eastern portion of the domain. Within large basins like the Missouri, positive groundwater contributions occur in the headwater regions and transitions to negative values downstream. This is an illustration of lateral groundwater convergence and regional flow systems. Note that results are mapped by subbasin, but all water balance

464 calculations are carried out for the complete watershed draining to a subbasin outlet.
465 Therefore, Fig. 3 should be viewed as a system of nested subbasins with values
466 representing progressively larger drainage areas as you move downstream. With this in
467 mind, it is also intuitive that some of the largest groundwater contribution ratios occur
468 in headwater basins while in downstream reaches on major rivers the values are smaller
469 indicating a regional balance between local groundwater surface water exchanges when
470 aggregating over larger drainage areas.
471
472 **2.4 Three approaches to evapotranspiration**
473 We have identified three common treatments of evapotranspiration within Budyko
474 analyses. As will be demonstrated later on, these three approaches are identical in
475 systems where the steady state assumption is valid and no storage changes are
476 occurring. However, when this is not the case, we hypothesize that the different
477 formulations for evapotranspiration will yield systematically different results. Here we
478 summarize the three approaches to E and how each approach is mimicked within the
479 simulated results.
480 Precipitation and runoff are generally much easier to measure at the watershed
481 scale than evapotranspiration or groundwater storage changes. As a result, in many
482 Budyko analyses evapotranspiration is not actually measured directly, but is calculated
483 as the difference between precipitation and surface outflow [e.g. *Greve et al.*, 2015;
484 *Jones et al.*, 2012; *Renner et al.*, 2014; *T Wang et al.*, 2009; *Xu et al.*, 2013; *Yang et al.*,
485 2009]. This approach relies on the assumption that changes in storage are negligible.
486 We refer to this as the *inferred evapotranspiration* approach and mimic it by
487 approximating the evapotranspiration ratio as simulated $(P- Q_{out})/P$. In other words, for
488 this approach, we disregard the simulated evapotranspiration values and generate a
489 new evapotranspiration estimate (i.e. the *inferred evapotranspiration*) indirectly from
490 the precipitation input to the model and the simulated overland flow. To be consistent
491 with other studies, we follow the standard assumption that storage changes are

492 negligible and do not include groundwater storage changes in this estimate. The
493 implications of this assumption are explored in the results section.
494 A more direct, if less common, approach is to quantify evapotranspiration from field
495 observations. This approach does not require a steady state assumption when
496 calculating evapotranspiration but it does require more rigorous field observations and
497 is therefore not feasible for Budyko analysis of data sparse areas. Within our simulation
498 results, however, 'data' is not a limitation. Our modeled outputs include gridded hourly
499 evapotranspiration for the entire domain. Simulated E values are aggregated by
500 watershed and used to represent the so called *direct evapotranspiration.* Note that in
501 this case we are still using simulated E not observations. The intention is to treat the
502 model as our synthetic truth and compare variations within this framework.
503 Finally, the most rigorous, and data intensive, approach is to quantify both
504 evapotranspiration and groundwater surface water exchanges directly. This approach
505 has been used in recent studies seeking to evaluate storage impacts on Budyko
506 relationships (e.g. *Istanbulluoglu et al.* [2012]; [*D Wang*, 2012]). Changes in
507 groundwater storage are not used to adjust evapotranspiration values directly but they
508 can be applied to precipitation estimates to better reflect the quantity of water that is
509 available to partition into overland flow or evapotranspiration. This is defined as
510 effective precipitation and is calculated as precipitation minus groundwater contribution
511 (*P-G)*. The effective precipitation approach was used by *Du et al.* [2016] in their study of
512 Budyko relationships in arid basins. For this study we mimic the effective precipitation
513 approach by using the simulated (or *direct*) evapotranspiration and combining the
514 model input precipitation with the calculated groundwater contributions. The
515 adjustment for effective precipitation within the Budyko framework is covered in
516 Section 2.5.
517 It should be noted here that the first two approaches (i.e. inferred and direct
518 evapotranspiration) are commonly used in analyses that rely on the standard
519 equilibrium assumption while the final method is designed for situations where this is
520 not the case. By comparing results between all three we consider the impact of nonzero

groundwater contributions both for approaches that assume it is negligible and that account for it.

2.5 Budyko analysis

Budykyo's original formulation expressed evapotranspiration ratio (E/P) as a function of aridity index (E_p/P) as follows [*Budyko*, 1974]:

$$\frac{E}{P} = \left\{ \frac{E_p}{P} \left[1 - \exp\left(-\frac{E_p}{P}\right) \tanh\left(\frac{P}{E_p}\right) \right] \right\}^{0.5} \quad (8)$$

Although the original analysis by Budyko did show some scatter around the curve, Eq. (8) defines a universal relationship that does not include any free parameters to account for spatial differences [*Budyko*, 1974]. Subsequent work has observed systematic variability between watersheds that can be related to climate, land cover and soil properties [e.g. *Donohue et al.*, 2007]. To reflect this, the original universal Budyko formulation has been refined multiple times to include additional free parameters [*Choudhury*, 1999; *Fu*, 1981; *Milly*, 1994; *L. Zhang et al.*, 2001; *L. Zhang et al.*, 2004]. For a summary of these formulations refer to *Du et al.* [2016] and *L. Zhang et al.* [2004] .

Here we apply the commonly used Budyko formulation from *Fu* [1981] and *L. Zhang et al.* [2004]:

$$\frac{E}{P} = 1 + \frac{E_p}{P} - \left(1 + \left(\frac{E_p}{P}\right)^{\omega}\right)^{1/\omega} \quad (9)$$

Eq. (9) includes one free parameter, ω which can range from one to infinity, henceforth referred to as the shape parameter. ω is an empirical parameter that has not been ascribed a specific physical meaning, but is generally conceptualized as an integrated catchment property that reflects characteristics such as land cover, soil properties, topography and seasonality [*L. Zhang et al.*, 2004]. If the evapotranspiration fraction and the aridity index are both known, ω can be calculated for any point on a Budyko plot using Eq. (9).

549 Fig. 4 plots Eq. (8) for a range of ω values. The bold line (ω=2.6) is roughly
550 equivalent to the original Budyko equation (Eq. 8) [*L. Zhang et al.*, 2004]. Following the
551 original Budyko assumption of no change in storage, in humid locations where potential
552 evaporation is less than precipitation, the system is energy limited and the maximum
553 value of E is E_p. Conversely, when the aridity index is greater than one the system is
554 water limited and the maximum E/P value is one (indicating that all incoming
555 precipitation is evaporated). As the shape parameter increases the curves moves
556 progressively closer to the water (E/P=1) and energy (E/P=E_p/P) limitations of the
557 system.
558 In the following sections, Budyko relationships are plotted and shape parameters
559 are evaluated for all three approaches using variations or Eq (9) as follows:
560 1. Inferred evapotranspiration: evapotranspiration is calculated from precipitation
561 and outflow so (P-Q_{out})/P is substituted for E/P in Eq. (9).
562 2. Direct evapotranspiration: Eq. (9) is applied as written.
563 3. Effective precipitation: precipitation is replaced by effective precipitation (P-G)
564 which means $E/(P\text{-}G)$ replaces E/P and $Ep/(P\text{-}G)$ replaces Ep/P in Eq (9).
565
566 **3. Results and discussion**
567 Results and discussion are divided into two sections. In section 3.1 the three approaches
568 to evapotranspiration fractions are compared across the entire simulation domain.
569 Systematic differences are identified and evaluated as a function of groundwater
570 contributions. A conceptual framework is presented to explain the biases between
571 approaches. In Section 3.2 the potential implications of these differences are illustrated
572 by comparing spatial patterns between the three approaches as well as relationships
573 across spatial scales.
574
575 **3.1 The impact of storage changes on Budyko Relationships**
576 Fig. 5 plots every watershed in the domain shown in Fig. 2 using the three
577 approaches to estimate the evapotranspiration fraction. In all three figures the

watershed points follow the overlaid Budyko curves; 77% of the watersheds fall within the 1.6 to 3.6 shape parameter lines for the inferred evapotranspiration approach, 51 % for the direct approach and 72% for the effective precipitation approach. This demonstrates that Budkyo relationships are recreated with the integrated hydrologic model. However, there are some notable differences between methods. With the inferred *E* approach shown in subplot a, the points are focused near the water limit line (i.e. (P- Q_{out}) /P=1) for high aridity values. Conversely, with the direct approach (subplot b), the evapotranspiration ratios are generally lower at high aridity values. Also, with the direct approach, there are points with evapotranspiration ratios greater than one and fall above the water limit. This would appear to violate the water balance and will be discussed more later.

Systematic differences between the Budyko plots shown in Fig. 5 are explained by the way groundwater contributions influence each approach. This is illustrated conceptually in Fig. 6. in systems with groundwater surface water interactions, incoming precipitation is equal to the sum of evapotranspiration, outflow and ground water contributions (Eq. (6)). This means that the difference between precipitation and outflow will only equal evapotranspiration if there are no storage changes (i.e. G is zero); if there are non-zero groundwater contributions then precipitation minus outflow is actually a measure of evapotranspiration plus groundwater contributions (and not the intended evapotranspiration). In other words, instead of evaluating,

$$\frac{E}{P} = f\left(\frac{E_p}{P}\right) \tag{10}$$

as intended in the Budyko formulation, the inferred evapotranspiration approach shown in Fig. 5a is actually plotting

$$\left(\frac{E}{P} + \frac{G}{P}\right) = f\left(\frac{E_p}{P}\right) \tag{11}$$

607 This is illustrated in Fig. 6a; the curve is now plotting the sum of the evapotranspiration
608 fraction and the groundwater contribution fraction, not the evapotranspiration fraction
609 for the original formulation shown in Fig. 4. The difference between the curve and the
610 limit lines in this case is still the outflow fraction though.
611 The direct evapotranspiration approach avoids the limitations of the inferred
612 approach by evaluating Budyo relationships as a function of the evapotranspiration
613 fraction as intended in Eq. (10). However, groundwater contributions will still bias the
614 results with this approach because the difference between precipitation and
615 evapotranspiration is outflow plus groundwater contribution (Eq. (6)). Thus, the curve in
616 Fig. 6b represents the evapotranspiration fraction (as with Fig. 4) but now the
617 partitioning is occurring between evaporation and runoff plus groundwater
618 contributions, not just runoff. This means that the maximum evapotranspiration fraction
619 (i.e. the upper water limit) is not one, but one minus the groundwater contribution
620 fraction.
621 This shift in the upper limits of water availability explains the values greater than
622 one in Fig. 5b; in these watersheds groundwater contributions are negative (i.e.
623 groundwater is supplying water to the land surface) and this allows for
624 evapotranspiration values that are greater than the incoming precipitation. Similar shifts
625 in the upper limits of the system for arid locations were found by *Potter and Zhang*
626 [2009] who noted that evapotranspiration was actually approaching a fixed portion of
627 potential evapotranspiration for high rainfall years in arid basins in Australia.
628 The effective precipitation approach is designed to maintain focus on
629 partitioning between evapotranspiration and overland flow by removing groundwater
630 contributions from the denominator of both ratios (i.e. adjusting both the x and y axes
631 in Fig. 6c) . This ensures that the modified outflow and evapotranspiration ratios will
632 sum to one even when groundwater surface water exchanges are occurring; to
633 accomplish this the modified ratios are expressed as a function of effective precipitation
634 not precipitation. It should also be noted from Fig. 6 that in the case where G is zero (i.e.
635 there are no storage changes), the three formulations are equivalent.

636 The systematic differences explained in Fig. 6 are evaluated by calculating the
637 shape parameter (Eq. (9)) for the curve corresponding to every watershed plotted in Fig.
638 5. Fig. 7 a-c plot the resulting shape parameters as a function of groundwater
639 contribution fraction colored by aridity for each of the three approaches. Recall from
640 Fig. 4 that larger curve numbers fall closer to the upper limits on the Budyko plots and
641 positive groundwater contribution fractions occur when there is a net flux from the
642 surface water to the groundwater (i.e. net infiltration). Positive G values are most
643 prevalent in the more arid western portions of the domain as is shown in Fig. 3d and
644 demonstrated by the shading in Fig. 7a-c where the most, red (arid) points occur further
645 to the right along the x axis. As would be expected from Fig. 6, Fig. 7. a-c illustrate
646 varying relationships between shape parameters and groundwater contributions for the
647 different approaches. Recall that all of the results are based on the same underlying
648 simulation so the differences in Fig. 7 result purely from accounting differences in how
649 the evapotranspiration fraction is calculated between approaches.
650 Both the inferred (6a) and direct approaches (6b) show clear, but contradictory,
651 relationships with groundwater surface water exchanges. There is a positive relationship
652 between the shape parameter and groundwater contribution fraction for the inferred
653 evapotranspiration approach at the lower limits of the system as delineated by the
654 dashed line in Fig. 7a. This indicates that in arid watershed watersheds, increased
655 groundwater contributions are correlated with larger evapotranspiration fraction (i.e.
656 with larger curve numbers). The behavior is consistent with Fig. 6a; because the
657 groundwater contribution is included in the evapotranspiration fraction when
658 evapotranspiration is inferred from precipitation and outflow (i.e. $P\text{-}Q_{out} = E + G$),
659 nonzero groundwater contributions vertically shift points in the Buydko plot.
660 Taking this idea further, Fig. 7d shows that a constant positive groundwater
661 contribution applied across aridity values will vertically shift the Budyko curve relative to
662 a scenario with no storage changes if evapotranspiration is inferred. In the case of a
663 positive groundwater contribution, this vertical shift moves points closer to the water
664 and energy limits of the system and therefore increases their shape parameters. Note

665 that in the Fu equation (Eq. (9)), Budyko curves with different shape parameter are not
666 parallel to one another and converge at low aridity values; therefore the same
667 groundwater contribution value changes the shape parameter differently depending on
668 the location within the Buyko plot. The linear trend traced along the lower portion of
669 the scatter plot in Fig. 7a shows that for the lowest curve numbers, occurring in
670 watersheds with high aridity, there is a roughly linear relationship between
671 groundwater contribution and shape parameters. This approximate linearity occurs
672 because the Fu curves become almost parallel for high aridity values (see Fig. 4). For
673 lower aridity values, this is not the case and the relationship between groundwater
674 contribution and shape parameter will be positive but nonlinear.
675 Fig. 7b plots groundwater contributions versus shape parameters similar to 6a
676 but for the direct evapotranspiration approach. Recall that with this approach the
677 groundwater contributions are now essentially lumped with the outflow fraction (as
678 opposed to the evapotranspiration fraction with the inferred approach, refer to Fig. 6a
679 and b). This means that rather than shifting points vertically in the Budyko plot (i.e. Fig.
680 7d), positive groundwater contributions change the total water that is available for
681 evapotranspiration. This can be conceptualized as shifting the limits of how much total
682 water is available for evapotranspiration.
683 In this case a positive groundwater contribution (i.e. surface water infiltrating to
684 groundwater) is essentially a loss to the surface water system and decreases the upper
685 limit of water available to the system. Fig. 7e illustrates this point for a constant
686 groundwater contribution across the entire Buydko plot. When groundwater
687 contributions are present the upper water limitation on the system shifts from 1 to 1-
688 G/P and the energy limitation shifts from E_p/P to E_p/P-G/P. However, if different
689 watersheds have varying levels of groundwater contribution this mean that each
690 watershed will now have a different upper limit; in other words, the evapotranspiration
691 fraction plus the outflow fraction is no longer always equal to one but rather one minus
692 the groundwater contribution fraction. This creates a nonlinear inverse relationship
693 between curve number and groundwater contributions. As the groundwater

694 contribution fraction increases, the decreasing upper bounds on evapotranspiration
695 fraction will bias the system towards lower curve numbers (refer to Fig. 4). This is a
696 nonlinear relationship which can be shown by calculating the shape parameter as a
697 function of groundwater contribution fraction in Eq. (9) for the limiting case where there
698 is no outflow (i.e. G/P=1-E/P). The dashed line on Fig. 7b shows the resulting
699 relationship for a relatively high aridity value of 6. The curve provides a good
700 approximation for the upper limit of Fig. 6b.
701 Finally, a scatter plot of shape parameters versus groundwater contribution
702 fraction for the effective precipitation case (Fig 6c) shows similar patterns with aridity
703 but no clear correlation between storage changes and shape parameters. This is to be
704 expected because the effective precipitation approach adjusts for groundwater
705 contributions in both the evapotranspiration ratios and the aridity index before plotting.
706 However, it should be noted that some dependence on groundwater contribution is still
707 to be expected the extent that groundwater surface water exchanges are also
708 correlated with other watershed properties. For example, groundwater contributions
709 levels can also be correlated with vegetation type, soil properties and other watershed
710 characteristics, which have been correlated to shape parameters in previous research
711 [e.g. *Li et al.*, 2013; *Shao et al.*, 2012; *Williams et al.*, 2012; *Xu et al.*, 2013; *Yang et al.*,
712 2009].
713 This is true for the other approaches too; while the effect of groundwater
714 contributions within each space can be precisely determined using Eq. (7) and Eq. (9), it
715 is important to note that the watersheds evaluated here are also heterogeneous in land
716 cover, topography and seasonality. Therefore, in the scatter plots shown in Fig. 7, the
717 relationships between shape parameters and groundwater contribution explained by
718 subplots d and e appear as limits rather than strong predictors. This point is also made
719 by *Istanbulluoglu et al.* [2012] who evaluated the impact of groundwater storage
720 changes on Budkyo relationships using the inferred evapotranspiration approach and
721 adjusting for storage changes using estimates from groundwater observations. They
722 provide a similar conceptual model to Fig. 7d describing consistent shifts within the

Buydko space as a function of groundwater contribution. However, for the four basins in Nebraska that they evaluated they found a negative relationship between inferred evapotranspiration ratios and aridity. This was attributed to a strong negative correlation between groundwater contribution fraction and aridity index. In other words, for this subset of basins, they show that the resulting trend is controlled by the dependence of groundwater contribution on other watershed characteristics.

Fig. 8 compares the shape parameters calculated with each approach to illustrate the way that different assumptions can bias derived Budyko relationships. Fig. 8a shows the differences between the inferred and direct evapotranspiration approaches, which are commonly used in studies that assume no change in storage. Because groundwater contributions are incorporated into different components of the water balance with these methods Fig. 8a shows that, for positive groundwater contributions (green points), the inferred shape parameters are systematically higher than the direct shape parameters, while the inverse is true when groundwater contributions are negative (purple points). Furthermore, when groundwater contributions are large (i.e. the dark green circles in subplot a), the direct method has uniformly low shape parameters, but the inferred method still shows a range of shape parameters. This is to be expected from the conceptual model of the direct evapotranspiration approach (Fig. 7e) where we showed that high groundwater contributions decrease the upper limit of the evapotranspiration ratio. This shift biases the system towards uniformly low shape parameters that are less sensitive to other watershed characteristics.

The direct and inferred evapotranspiration methods are also compared to the effective precipitation approach, which does account for groundwater contributions (Fig.7 b &c). As would be expected, the direct and inferred approaches have inverse biases relative to the effective precipitation method; shape parameters are systematically higher with the inferred approach relative effective precipitation and lower for the direct approach. Here too the trends with groundwater contributions are reversed with positive contributions creating a positive bias for the inferred case and a

752 negative bias for the effective precipitation case. This result is in keeping with the
753 conceptual model of groundwater contributions to each approach; with the inferred
754 evapotranspiration approach groundwater contributions are lumped with
755 evapotranspiration while in the direct approach they are lumped with outflows.
756 Also, there is a much stronger correlation between the inferred
757 evapotranspiration and effective precipitation approaches (Fig. 8b) than between direct
758 evapotranspiration and effective evapotranspiration approaches (Fig. 8c) (r^2 value of
759 0.96 comparing inferred vs. effective as opposed to 0.32 for inferred vs. direct). This is
760 partially due to the lack of sensitivity of shape parameters in the direct approach when
761 groundwater contributions are large, as was previously noted and is also illustrated in
762 Fig. 8a. For all three cases, Fig. 8 demonstrates systematic variability in the shape
763 parameter even for relatively small groundwater contributions. As with Fig. 7, Fig 8
764 there is still significant scatter in each of these comparisons. In this case the scatter is
765 caused by the fact that the shape parameter will be impacted (1) by how large the
766 groundwater contribution fraction is and (2) the aridity of the watershed. Groundwater
767 contributions shift points within the Budyko plot in a linear fashion (although the
768 direction varies according to the approach) but the resulting change in shape parameter
769 will have a nonlinear dependence on both aridity and evapotranspiration fraction.
770
771 **3.2 Spatial patterns and scaling**
772 Section 3.1 explored the relationship between groundwater storage and shape
773 parameters using the three different approaches to evapotranspiration fractions. Here,
774 we illustrate the impacts of these differences on spatial patterns in shape parameters
775 and scaling relationships. The intent is to provide a demonstration of how systematic
776 differences will propagate across spatial scales using the 1985 simulation as a test case.
777 Obviously local differences will vary depending on the time period used for analysis and
778 the associated levels of groundwater contribution.
779 Fig. 9 maps shape parameters for all of the roughly 33,000 nested watersheds in
780 the simulation domain calculated using the three different approaches to

781 evapotranspiration ratios. Even though the one-year transient simulation used for the
782 analysis presented does not meet the Budyko equilibrium criteria, Figs. 4c and 8c show
783 that realistic Budyko relationships are still found when groundwater contributions are
784 accounted for using the effective precipitation approach. *Xu et al.* [2013] built a neural
785 network model to predict shape parameters using long-term observations from 224
786 watersheds with drainage areas ranging from 100 to 10,000 km^2. They then predicted
787 shape parameters globally using a variety of catchment characteristics. Excluding the
788 small drainage areas with shape parameters greater than four, the spatial patterns
789 calculated here with the effective precipitation approach (i.e. the only approach that
790 corrects for groundwater contributions, Fig. 9c) match well with the global map
791 presented by *Xu et al.* [2013].
792 All three maps demonstrate local variability and regional trends in the shape
793 parameters. This spatial variability is partially caused by the spatial patterns in
794 groundwater contribution fraction shown in Fig. 3d; however, it is also a reflection of
795 variability in catchment characteristics such as vegetative properties, topography and
796 climate that have been correlated to Budyko relationships by previous studies[e.g. *Li et*
797 *al.*, 2013; *Milly*, 1994; *Shao et al.*, 2012; *Williams et al.*, 2012; *Xu et al.*, 2013; *Yang et al.*,
798 2009; *Yokoo et al.*, 2008]. The purpose here is not to isolate all of the sources of spatial
799 heterogeneity, rather to illustrate how spatial patterns change depending on the
800 treatment of storage.
801 Spatial patterns are consistent between the three approaches in the more humid
802 eastern portion of the domain, where groundwater contribution ratios are generally
803 smaller (Fig. 3d), but in the more arid western portion of the domain significant
804 differences are observed. For both the inferred evapotranspiration and effective
805 precipitation approaches there are large red areas indicating shape parameters greater
806 than four where the evapotranspiration ratio is falling very close to the water limitation.
807 The areas with the highest shape parameters (i.e. greater than four) are generally
808 consistent between the inferred evapotranspiration and effective precipitation
809 approaches, but the inferred approach results in higher curve numbers throughout the

western portion of the domain than the effective precipitation approach. This is consistent with Fig. 8b that showed strong correlations between the shape parameters of these two approaches (r^2=0.96) but a slight positive bias with positive groundwater contributions for the inferred evapotranspiration approach; 62% of watersheds overall and 86% of watersheds with a positive groundwater contribution have a higher shape parameter using the inferred evapotranspiration approach..

Conversely, with the direct evapotranspiration approach the western portion of the domain has much lower shape parameters and less spatial variability. Again, this finding is consistent with Fig. 7b and e, which show that when groundwater contributions are high, the curve numbers are uniformly low because the flux from the surface water system to the groundwater shifts the upper limit of the evapotranspiration fraction down. The systematic differences in Fig. 9, both with respect to the shape parameter values and the spatial patterns in these parameters, where groundwater surface water exchanges are occurring indicate the potential to arrive at fundamentally different conclusions about spatial trends in shape parameters depending on the approach used.

Next, we evaluate groundwater impacts a function of drainage area. Budyko originally limited analysis to large basins (which he defined as drainage areas greater than 10,000 km^2) where he argued that macroclimate can be expected to dominate partitioning [*Budyko*, 1974]. Indeed subsequent work has shown that for smaller areas vegetation dynamics become increasingly important [*Donohue et al.*, 2007]. Fig. 10 plots Budyko relationships for every watershed grouped by drainage area using the effective precipitation formulation as an example. In this figure, the drainage area is increased from watersheds less than 1,000 km^2 (9a) to watersheds greater than 100,000 km^2 (9d). This figure shows that the scatter decreases as drainage area increases and the points converge around a single curve. This behavior illustrates increased importance of local watershed characteristics for smaller drainage areas consistent with previous studies [e.g. *Budyko*, 1974; *Donohue et al.*, 2007]. We do not show the other

838 two approaches for this example because similar convergence behavior with larger
839 drainage areas is found in all three cases.
840 The shape parameters estimated with the effective precipitation approach are
841 arguably the most comparable to other long-term studies that have assumed
842 equilibrium conditions (assuming that the watersheds they studied actually were in
843 equilibrium over the study period). The simulated median value found here is slightly
844 lower than the original Budyko value of 2.6 and the median value of 2.56 found by
845 [*Greve et al.*, 2015] using the 411 Model Parameter Estimation Experiment (MOPEX)
846 catchments in the US. However, it compares well with 1.8 median value for large
847 MOPEX basins in the US reported by *Xu et al.* [2013]; although, it should be noted that
848 *Xu et al.* [2013] report a higher 2.6 median value for small basins, and the median small
849 basin value reported found here is 2.0. Part of this bias can likely be attributed to the
850 concentration of MOPEX basins in the eastern portion of the US where Fig. 9 shows that
851 shape parameters are generally higher. Overall, the consistency in spatial patterns and
852 convergence around the Budkyo curve for large drainage areas indicates that the
853 ParFlow-CLM model recreates Budyko relationships even over a relatively short annual
854 simulation period as long as groundwater contributions are adjusted for (i.e. using the
855 effective precipitation approach). However, for smaller watersheds variability in
856 catchment characteristics is still an important consideration.
857 While all three approaches have decreased variance with increased drainage
858 area, the median and variance are not necessarily consistent between methods. Fig. 11
859 shows the interquartile range of shape parameters for each approach with increasing
860 drainage area. In all three cases, the 75^{th} percentile shape parameters decrease and the
861 25^{th} percentile shape parameter increases with increasing area. Again this indicates
862 increased importance of watershed characteristics at smaller scales; local variability is
863 muted and the probability of observing very high or very low shape parameters
864 decreases as the scale increases from smaller to larger watersheds. In the case of the
865 inferred and direct evapotranspiration approaches, because groundwater contributions
866 are not accounted for in the calculations, some of this variability can also be attributed

867 to spatial patterns in groundwater surface water exchanges and lateral groundwater
868 flow. As previously noted, the groundwater contribution map (Fig. 3d) shows that the
869 largest, positive or negative, groundwater contribution fractions generally occur in small
870 headwater basins. Across larger areas, local groundwater surface water exchanges
871 balance out and the overall groundwater contribution fractions for large watersheds
872 tend to be smaller.
873 Consistent with Figs. 7 and 8, the inferred evapotranspiration and effective
874 precipitation approaches are the most similar. For the largest drainage areas, the
875 median shape parameter is 1.8 for the inferred evapotranspiration approach, 1.5 for the
876 direct evapotranspiration approach and 1.7 using effective precipitation. The direct
877 evapotranspiration formulation has systematically lower shape parameters than the
878 other two approaches; the median value for this method is consistently below the other
879 two. Again this agrees with section 3.1 where we demonstrated an inverse relationship
880 between shape parameters and groundwater contributions. The direct
881 evapotranspiration approach also has a consistently smaller interquartile range than the
882 other two methods. This results from the negative correlation with groundwater
883 contribution and the decreased sensitivity that was shown for small shape parameters
884 in arid locations. Fig. 11 shows that all three approaches will yield qualitatively similar
885 scaling relationships and convergence for large basins; however, the shape parameter
886 values will vary.
887
888 **4. Conclusions**
889 One of the primary assumptions of the Buydko hypothesis is that watersheds are
890 in equilibrium and there are no changes in storage. This means that all incoming
891 precipitation will either leave the watershed as evapotranspiration or overland flow.
892 While the original Budyko curve has been well verified with observations from around
893 the globe, it is also now widely accepted that the relationship between
894 evapotranspiration ratios and aridity indices is not universal and some additional curve
895 parameters are needed to account for spatial variability between watersheds. Many

subsequent studies have related curve parameters to catchment properties such as vegetation, topography and seasonality [e.g. *Li et al.*, 2013; *Shao et al.*, 2012; *Williams et al.*, 2012; *Xu et al.*, 2013; *Yang et al.*, 2009]. More recently, additional studies have shown that if groundwater surface water exchanges are present this can also influence the shape of the curve and account for additional variability between watersheds [*Milly and Dunne*, 2002; *Lu Zhang et al.*, 2008].

While methods have been developed to account for storage changes within the Budyko framework [e.g. *Du et al.*, 2016], very few studies have sufficient data on groundwater surface water interactions to evaluate the validity of the equilibrium assumption, much less to precisely quantify storage changes in their analysis. One of the key advantages of the Budyko approach is its ability to predict behavior based on a small number of relatively easy to obtain observations. Given its common application to data sparse watersheds, where even evapotranspiration measurements are often not available, directly quantifying groundwater surface water exchanges in these locations seems unlikely. Therefore, it is important to understand the sensitivity of Budyko relationships to uncertainty in storage changes in a general context that can be used to interpret results were precise measurements are not available.

Previous work has demonstrated systematic shifts in Budyko plots caused by groundwater surface water interactions [*Du et al.*, 2016; *Istanbulluoglu et al.*, 2012; *Milly and Dunne*, 2002; *D Wang*, 2012; *L. Zhang et al.*, 2004]. Here we demonstrate that the influence of groundwater storage changes on Budyko results will vary depending on how evapotranspiration is handled in the study. If evapotranspiration is measured directly, positive groundwater contributions (i.e. net infiltration from the surface to the subsurface) shift shape parameters down; conversely, if evapotranspiration is estimated using precipitation and runoff positive groundwater contributions will increase shape parameters. In both cases the sensitivity of the shape parameter to storage changes varies non-linearly with both the aridity of the watershed and the evapotranspiration fraction.

Using a one-year simulation with an integrated hydrologic model we demonstrate these differences can result in different conclusions about spatial patterns in Budyko relationships and the median shape parameter across spatial scales. This indicates that it is important to consider the approach used for estimating evapotranspiration fractions when comparing results between studies, and provides a demonstration of the types of bias that would be expected if different methods are used.

These results also have implications for the myriad of studies that seek to relate shape parameters for Buydko curves to other watershed characteristics. The conceptual models shown here illustrate that groundwater contributions will shift points in consistent and predictable ways when other variables are held constant (i.e. if you apply a consistent groundwater contribution across the entire range of aridity values or consider the shift of a single point with a given aridity value). However, we use the results from our integrated hydrologic model to demonstrate that that within complex heterogeneous domains groundwater surface water exchanges are spatially heterogeneous and depend on watershed characteristics such as aridity values, which can also influence Budyko relationships. The scatter in Figs. 6 and 7 demonstrate that groundwater contributions cannot easily serve as an independent predictor of the shape of Budyko relationships. This also shows that in large comparative studies, the bias caused by groundwater surface water interactions may not be readily apparent because it will vary from watershed to watershed.

The intention of these comparisons is not to discredit previous approaches, rather to illustrate the potential impacts of assuming equilibrium conditions across a broad range of physiographic settings and spatial scales without the ability to verify this assumption. Our results show that even when changes in storage are occurring, large watersheds still roughly follow Budyko curve; however the shape parameter and scatter will vary with groundwater contribution and depending on how evapotranspiration is quantified. We suggest that studies that cannot verify the equilibrium assumption using groundwater observations include additional analysis to evaluate the sensitivity of

their findings to uncertainty in storage changes by perturbing points using the conceptual models presented here. Even if groundwater contributions cannot be directly incorporated into analyses, this can help determine whether differences in shape parameters are actually resulting from unique basin characteristics or uncertainty in storage.

Data Availability:

All data from this analysis are available upon request. Instructions for accessing the ParFlow simulations used here are provided in [*Maxwell et al.*, 2016].

Acknowledgements:

Funding for this work was provided by the US Department of Energy Office of Science, Offices of Advanced Scientific Computing Research and Biological and Environmental Sciences IDEAS project. The ParFlow simulations were also made possible through high-performance computing support from Yellowstone (ark:/85065/d7wd3xhc) provided by National Center for Atmospheric Research's Computational and Information Systems Laboratory, sponsored by the National Science Foundation.

971 **Works Cited**

972 Barnes, M. L., C. Welty, and A. J. Miller (2016), Global Topographic Slope Enforcement to
973 Ensure Connectivity and Drainage in an Urban Terrain, Journal of Hydrologic
974 Engineering, 21(4), 06015017, doi: doi:10.1061/(ASCE)HE.1943-5584.0001306.

975 Budyko, M. I. (1958), The Heat Balance of the Earth's Surface*Rep.*, 140-161 pp, U.S.
976 Department of Commerce, Weather Bureau, Washington D.C.

977 Budyko, M. I. (1974), Climate and LIfe, Academic Press, New York.

978 Choudhury, B. (1999), Evaluation of an empirical equation for annual evaporation using
979 field observations and results from a biophysical model, Journal of Hydrology, 216(1–2),
980 99-110, doi: http://dx.doi.org/10.1016/S0022-1694(98)00293-5.

981 Condon, L. E., A. S. Hering, and R. M. Maxwell (2015), Quantitative assessment of
982 groundwater controls across major US river basins using a multi-model regression
983 algorithm, Advances in Water Resources, 82, 106-123, doi:
984 http://dx.doi.org/10.1016/j.advwatres.2015.04.008.

985 Cosgrove, B. A., et al. (2003), Real-time and retrospective forcing in the North American
986 Land Data Assimilation System (NLDAS) project, J. Geophys. Res., 108(D22), doi:
987 10.1029/2002JD003118.

988 Dai, Y., et al. (2003), The Common Land Model, Bulletin of the American Meterorological
989 Society, 84(8), 1013-1023, doi: 10.1175/BAMS-84-8-1013.

990 Donohue, R. J., M. L. Roderick, and T. R. McVicar (2007), On the importance of including
991 vegetation dynamics in Budyko's hydrological model, Hydrol. Earth Syst. Sci., 11(2), 983-
992 995, doi: 10.5194/hess-11-983-2007.

993 Donohue, R. J., M. L. Roderick, and T. R. McVicar (2011), Assessing the differences in
994 sensitivities of runoff to changes in climatic conditions across a large basin, Journal of
995 Hydrology, 406(3–4), 234-244, doi: http://dx.doi.org/10.1016/j.jhydrol.2011.07.003.

996 Du, C., F. Sun, J. Yu, X. Liu, and Y. Chen (2016), New interpretation of the role of water
997 balance in an extended Budyko hypothesis in arid regions, Hydrol. Earth Syst. Sci., 20(1),
998 393-409, doi: 10.5194/hess-20-393-2016.

999 Ferguson, I. M., J. L. Jefferson, R. M. Maxwell, and S. J. Kollet (2016), Effects of root
1000 water uptake formulation on simulated water and energy budgets at local and basin
1001 scales, Environmental Earth Sciences, 75(4), 1-15, doi: 10.1007/s12665-015-5041-z.

1002 Fu, B. P. (1981), On the calculation of the evaporation from land surface (in Chinese),
1003 Sci. Atmos. Sin., 5, 23-31.

1004 Gentine, P., P. D'Odorico, B. R. Lintner, G. Sivandran, and G. Salvucci (2012),
1005 Interdependence of climate, soil, and vegetation as constrained by the Budyko curve,
1006 Geophysical Research Letters, 39(19), n/a-n/a, doi: 10.1029/2012GL053492.

1007 Gleeson, T., L. Smith, N. Moosdorf, J. Hartmann, H. H. Durr, A. H. Manning, L. P. H. van
1008 Beek, and A. M. Jellinek (2011), Mapping permeability over the surface of the Earth,
1009 Geophysical Research Letters, 38(L02401), doi: 10.1029/2010GL045565.

1010 Greve, P., L. Gudmundsson, B. Orlowsky, and S. I. Seneviratne (2015), Introducing a
1011 probabilistic Budyko framework, Geophysical Research Letters, 42(7), 2261-2269, doi:
1012 10.1002/2015GL063449.

1013 Istanbulluoglu, E., T. Wang, O. M. Wright, and J. D. Lenters (2012), Interpretation of
1014 hydrologic trends from a water balance perspective: The role of groundwater storage in
1015 the Budyko hypothesis, Water Resources Research, 48(3), n/a-n/a, doi:
1016 10.1029/2010WR010100.

1017 Jefferson, J. L., and R. M. Maxwell (2015), Evaluation of simple to complex
1018 parameterizations of bare ground evaporation, Journal of Advances in Modeling Earth
1019 Systems, 7(3), 1075-1092, doi: 10.1002/2014MS000398.

1020 Jones, J. A., I. F. Creed, K. L. Hatcher, R. J. Warren, M. B. Adams, M. H. Benson, E. Boose,
1021 W. A. Brown, J. L. Campbell, and A. Covich (2012), Ecosystem processes and human
1022 influences regulate streamflow response to climate change at long-term ecological
1023 research sites, BioScience, 62(4), 390-404.

1024 Kollet, S. J., and R. M. Maxwell (2006), Integrated surface–groundwater flow modeling:
1025 A free–surface overland flow boundary condition in a parallel groundwater flow model,
1026 Advances in Water Resources, 29(7), 945-958, doi: 10.1016/j.advwatres.2005.08.006.

1027 Kollet, S. J., and R. M. Maxwell (2008), Capturing the influence of groundwater dynamics
1028 on land surface processes using an integrated, distributed watershed model, Water
1029 Resources Research, 44(W02402), doi: 10.1029/2007WR006004.

1030 Koster, R. D., and M. J. Suarez (1999), A Simple Framework for Examining the
1031 Interannual Variability of Land Surface Moisture Fluxes, Journal of Climate, 12(7), 1911-
1032 1917, doi: doi:10.1175/1520-0442(1999)012<1911:ASFFET>2.0.CO;2.

1033 Li, D., M. Pan, Z. Cong, L. Zhang, and E. Wood (2013), Vegetation control on water and
1034 energy balance within the Budyko framework, Water Resources Research, 49(2), 969-
1035 976, doi: 10.1002/wrcr.20107.

1036 Maxwell, R. M. (2013), A terrain-following grid transform for parallel, large-scale,
1037 integrated hydrologic modeling, Advances in Water Resources, 53, 109-117, doi:
1038 10.1016/j.advwatres.2012.10.001.

1039 Maxwell, R. M., and N. L. Miller (2005), Development of a coupled land surface and
1040 groundwater model, Joural of Hydrometerology, 6(3), 233-247, doi:
1041 doi:10.1175/JHM422.1.

1042 Maxwell, R. M., and L. E. Condon (2016), Connections between groundwater flow and
1043 transpiration partitioning, Science, 353(6297), 377-380, doi: DOI:
1044 10.1126/science.aaf7891.

1045 Maxwell, R. M., L. E. Condon, and S. J. Kollet (2015), A high resolution simulation of
1046 groundwater and surface water over most of the continental US with the integrated
1047 hydrologic model ParFlow v3, Geoscientific Model Development, 8, 923-937, doi:
1048 10.5194/gmd-8-1-2015.

1049 Maxwell, R. M., L. E. Condon, S. J. Kollet, K. Maher, R. Haggerty, and M. M. Forrester
1050 (2016), The imprint of climate and geology on the residence times of groundwater,
1051 Geophysical Research Letters, 43(2), 701-708, doi: 10.1002/2015GL066916.

1052 Milly, P. C. D. (1994), Climate, soil water storage, and the average annual water balance,
1053 Water Resources Research, 30(7), 2143-2156, doi: 10.1029/94WR00586.

1054 Milly, P. C. D., and K. A. Dunne (2002), Macroscale water fluxes 2. Water and energy
1055 supply control of their interannual variability, Water Resources Research, 38(10), 24-21-
1056 24-29, doi: 10.1029/2001WR000760.

1057 Mitchell, K. E., et al. (2004), The multi-institution North American Land Data Assimilation
1058 System (NLDAS): Utilizing multiple GCIP products and partners in a continental
1059 distributed hydrological modeling system, J. Geophys. Res., 109(D07S90), doi:
1060 10.1029/2003JD003823.

1061 Potter, N. J., and L. Zhang (2009), Interannual variability of catchment water balance in
1062 Australia, Journal of Hydrology, 369(1–2), 120-129, doi:
1063 http://dx.doi.org/10.1016/j.jhydrol.2009.02.005.

1064 Renner, M., K. Brust, K. Schwärzel, M. Volk, and C. Bernhofer (2014), Separating the
1065 effects of changes in land cover and climate: a hydro-meteorological analysis of the past
1066 60 yr in Saxony, Germany, Hydrol. Earth Syst. Sci., 18(1), 389-405, doi: 10.5194/hess-18-
1067 389-2014.

1068 Shao, Q., A. Traylen, and L. Zhang (2012), Nonparametric method for estimating the
1069 effects of climatic and catchment characteristics on mean annual evapotranspiration,
1070 Water Resources Research, 48(3), n/a-n/a, doi: 10.1029/2010WR009610.

1071 Troch, P. A., G. Carrillo, M. Sivapalan, T. Wagener, and K. Sawicz (2013), Climate-
1072 vegetation-soil interactions and long-term hydrologic partitioning: signatures of
1073 catchment co-evolution, Hydrol. Earth Syst. Sci., 17(6), 2209-2217, doi: 10.5194/hess-
1074 17-2209-2013.

1075 Van Genuchten, M. T. (1980), A Closed-form Equation for Predicting the Hydraulic
1076 Conductivity of Unsaturated Soils, Soil Science Society of America, 44(5), 892-898.

1077 Wang, D. (2012), Evaluating interannual water storage changes at watersheds in Illinois
1078 based on long-term soil moisture and groundwater level data, Water Resources
1079 Research, 48(3), n/a-n/a, doi: 10.1029/2011WR010759.

1080 Wang, T., E. Istanbulluoglu, J. Lenters, and D. Scott (2009), On the role of groundwater
1081 and soil texture in the regional water balance: An investigation of the Nebraska Sand
1082 Hills, USA, Water Resources Research, 45(10), n/a-n/a, doi: 10.1029/2009WR007733.

1083 Williams, C. A., et al. (2012), Climate and vegetation controls on the surface water
1084 balance: Synthesis of evapotranspiration measured across a global network of flux
1085 towers, Water Resources Research, 48(6), n/a-n/a, doi: 10.1029/2011WR011586.

1086 Xu, X., W. Liu, B. R. Scanlon, L. Zhang, and M. Pan (2013), Local and global factors
1087 controlling water-energy balances within the Budyko framework, Geophysical Research
1088 Letters, 40(23), 6123-6129, doi: 10.1002/2013GL058324.

1089 Yang, D., F. Sun, Z. Liu, Z. Cong, G. Ni, and Z. Lei (2007), Analyzing spatial and temporal
1090 variability of annual water-energy balance in nonhumid regions of China using the
1091 Budyko hypothesis, Water Resources Research, 43(4), n/a-n/a, doi:
1092 10.1029/2006WR005224.

1093 Yang, D., W. Shao, P. J. F. Yeh, H. Yang, S. Kanae, and T. Oki (2009), Impact of vegetation
1094 coverage on regional water balance in the nonhumid regions of China, Water Resources
1095 Research, 45(7), n/a-n/a, doi: 10.1029/2008WR006948.

1096 Yokoo, Y., M. Sivapalan, and T. Oki (2008), Investigating the roles of climate seasonality
1097 and landscape characteristics on mean annual and monthly water balances, Journal of
1098 Hydrology, 357(3–4), 255-269, doi: http://dx.doi.org/10.1016/j.jhydrol.2008.05.010.

1099 Zhang, L., W. R. Dawes, and G. R. Walker (2001), Response of mean annual
1100 evapotranspiration to vegetation changes at catchment scale, Water Resources
1101 Research, 37(3), 701-708, doi: 10.1029/2000WR900325.

1102 Zhang, L., N. Potter, K. Hickel, Y. Zhang, and Q. Shao (2008), Water balance modeling
1103 over variable time scales based on the Budyko framework – Model development and
1104 testing, Journal of Hydrology, 360(1–4), 117-131, doi:
1105 http://dx.doi.org/10.1016/j.jhydrol.2008.07.021.

1106 Zhang, L., K. Hickel, W. R. Dawes, F. H. S. Chiew, A. W. Western, and P. R. Briggs (2004),
1107 A rational function approach for estimating mean annual evapotranspiration, Water
1108 Resources Research, 40(2), n/a-n/a, doi: 10.1029/2003WR002710.
1109

1110

Figures:

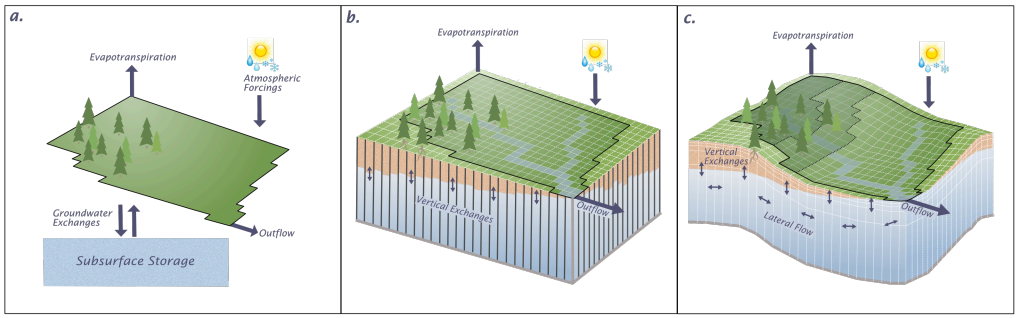

Figure 1: Conceptual illustration of (a) lumped parameter hydrologic models, (b) land surface models with vertical subsurface exchanges and (c) integrated hydrologic models. The nested subbasin approach is also illustrated on subplot c using the black outlines for reference.

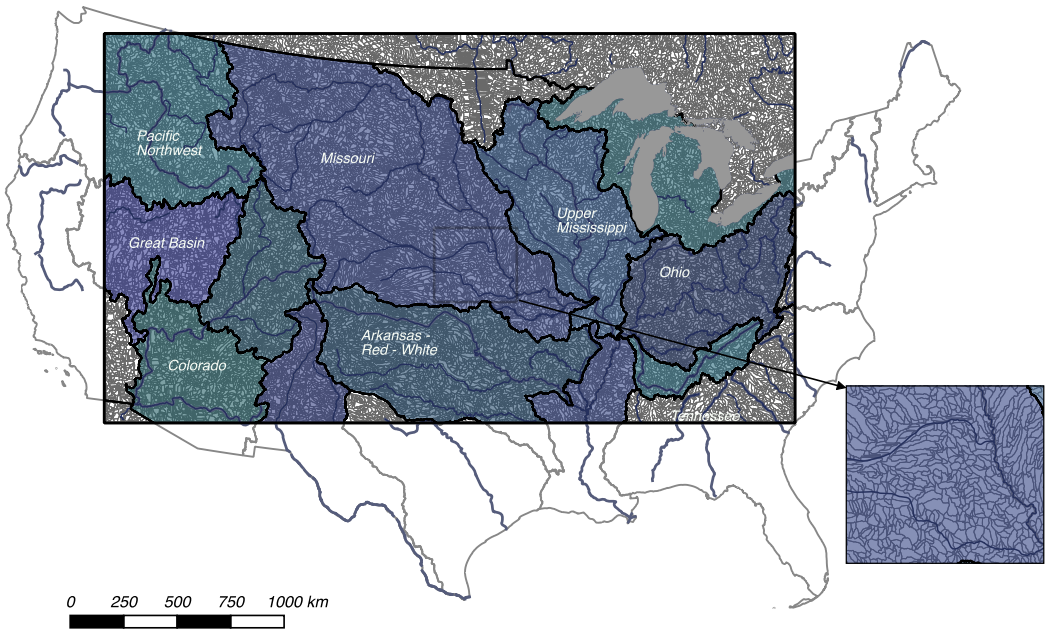

Figure 2: Map of the simulation domain extent (black box) with major river basins highlighted and labeled. Subbasins within the domain are outlined in grey. Major rivers are show in blue for reference (Note that the simulated river network is much more highly resolved as illustrated in [*Maxwell et al.*, 2015])

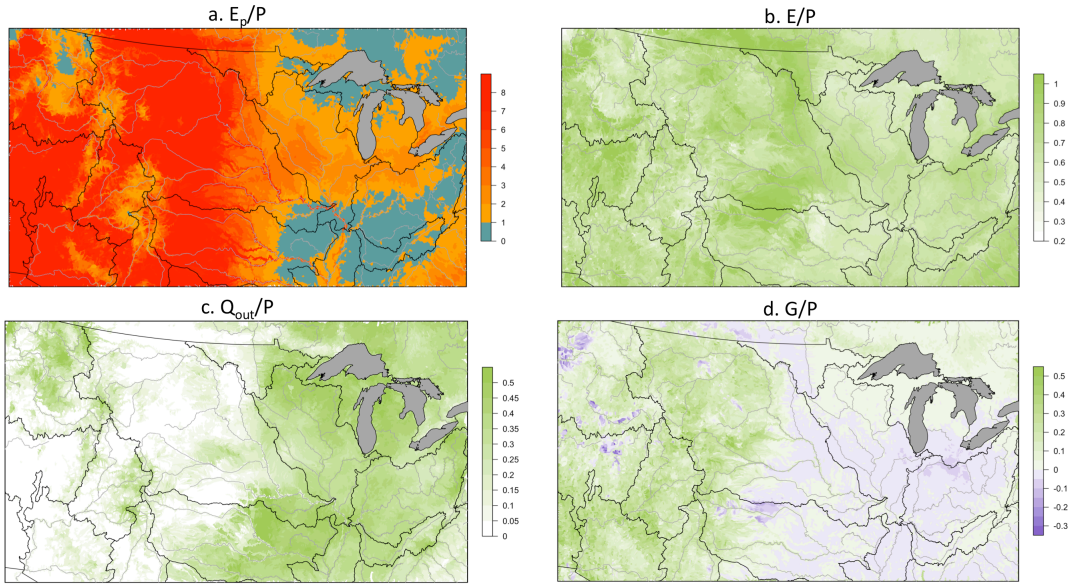

Figure 3: Maps of (a) aridity index (Ep/P) and the ratios of (b) evapotranspiration (c) outflow and (d) groundwater contributions (G/P) compared to precipitation. Major river basins are outlined in black. Note that ratios are mapped according to the subbasins shown in Fig. 2 but the values reflect the water balance for the entire watershed. This is a system of nested watersheds so the value for each watershed is reported at its outlet subbasin.

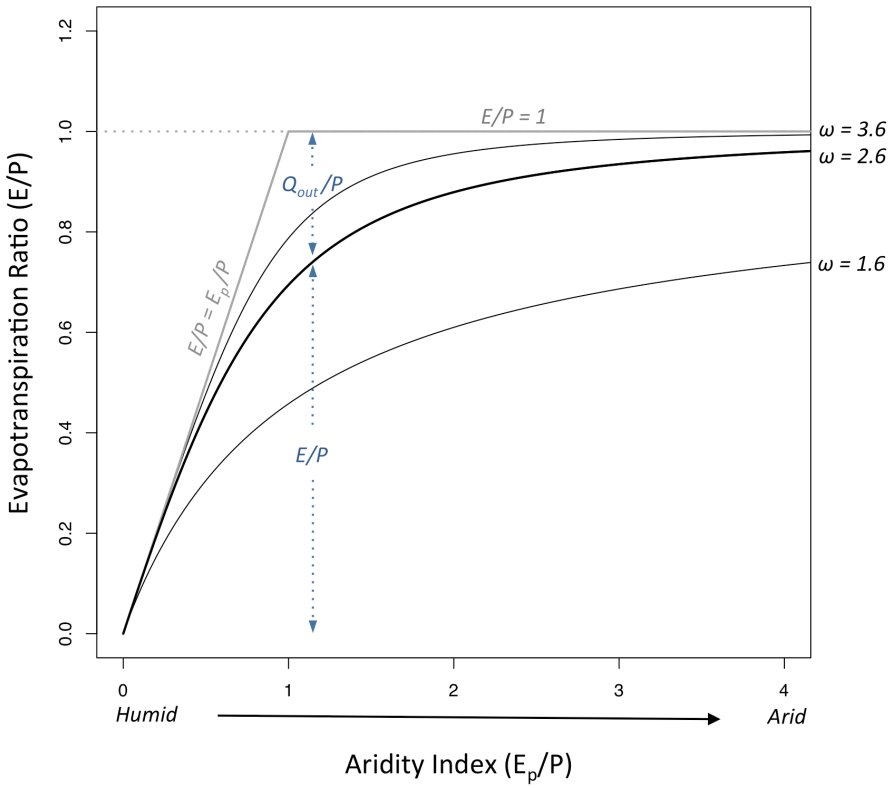

1134

1135 **Figure 4:** Illustration of the Budkyo framework showing curves with three different

1136 shape parameters (black lines, ω=1.6, 2.6 and 3.6) in relation to the water (E/P=1) and

1137 energy ($E/P=E_p/P$) limits of the system, grey lines.

1138

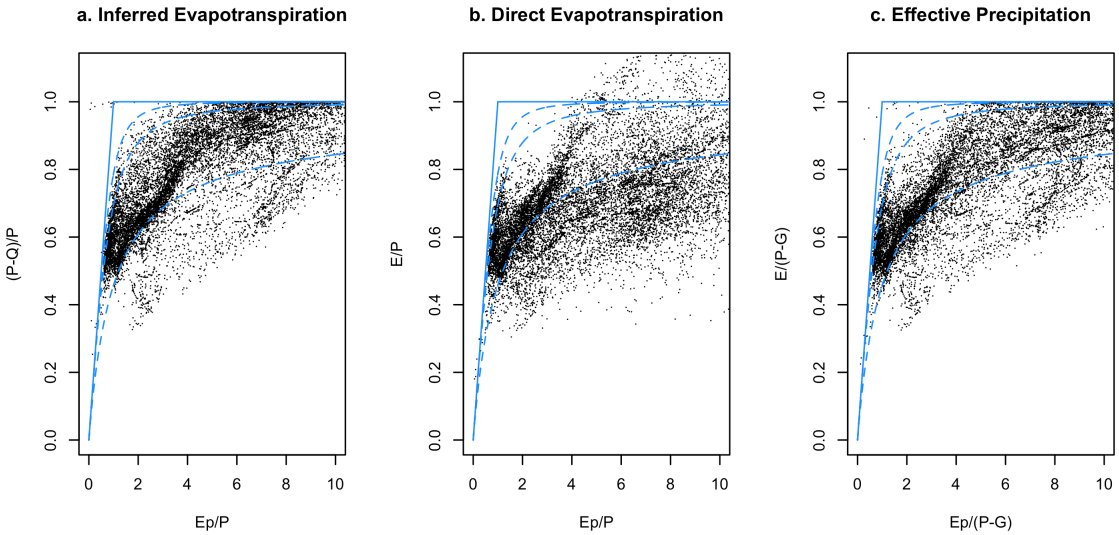

Figure 5: Budyko plots for the three approaches (a) inferred evapotranspiration, (b) direct evapotranspiration and (c) effective precipitation with points for every watershed in the domain. Dashed blue lines are Budkyko curves with ω values of 1.6, 2.6 and 3.6 and the solid blue lines are the water and energy limits (refer to Fig. 4).

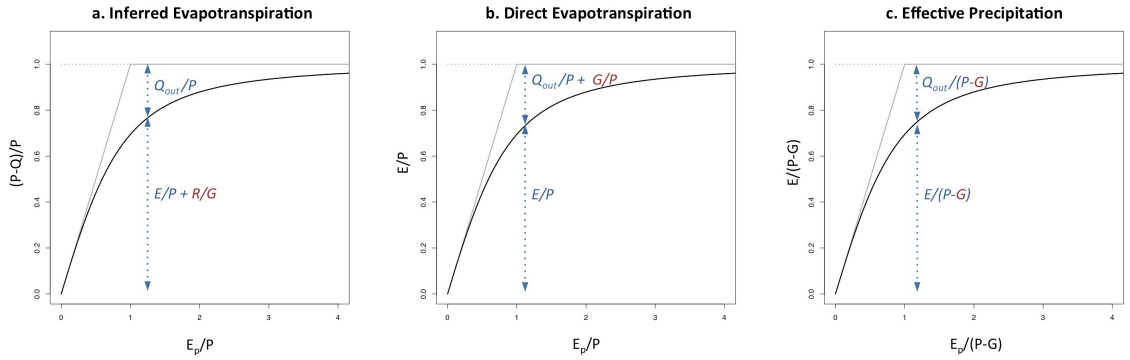

Figure 6: Illustration of the treatment of groundwater contributions for each of the three approaches. The black lines show the water and energy limits and an example Budyko curve, similar to Fig. 4. Arrows indicate the water balance component represented above and below the curve in each case.

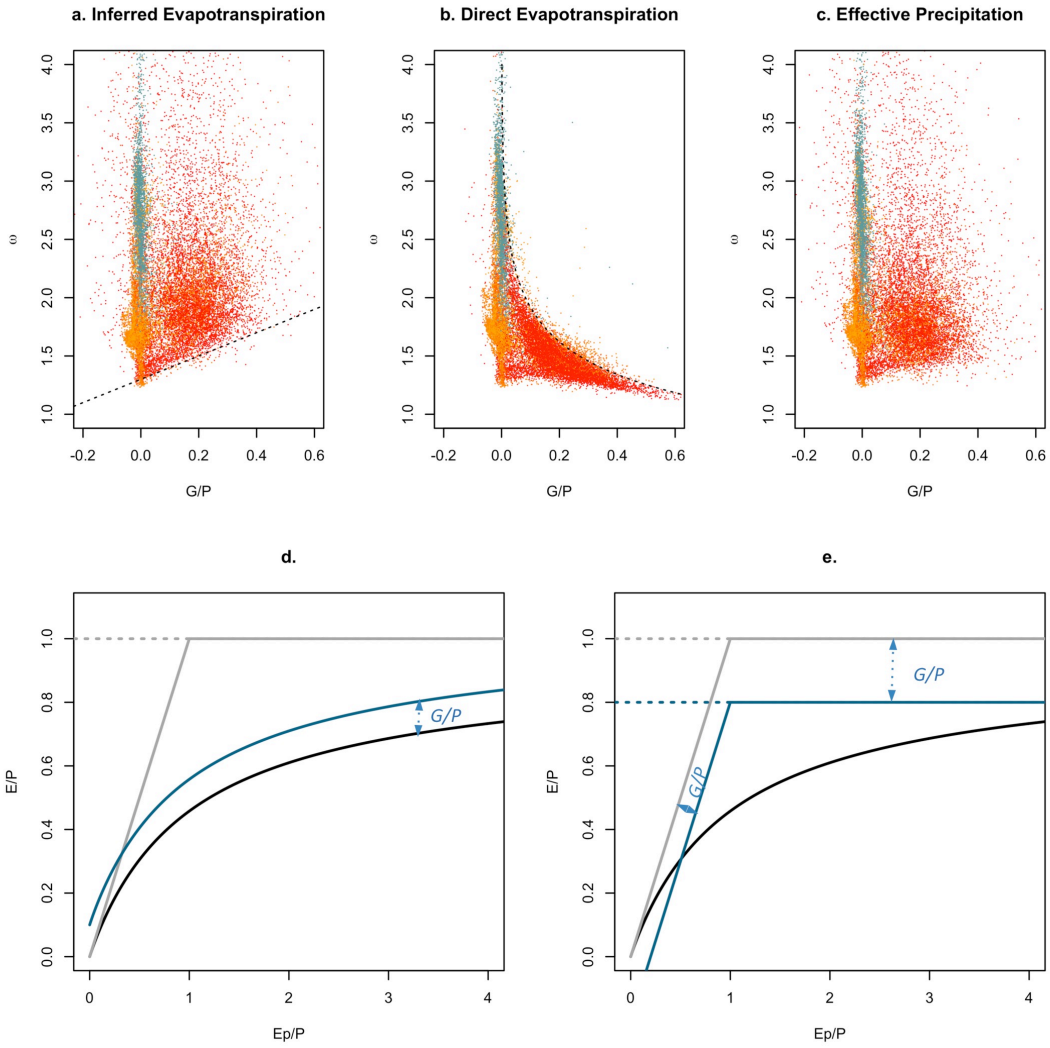

Figure 7: Comparison of shape parameters to groundwater contribution ratios for the three approaches in every watershed (a-c). Points are colored by aridity as shown in Fig. 3a. A dashed line with a slope of one is included on (a) for reference. The dashed line on (b) shows the relationship between the shape parameter and groundwater contribution fraction for an example aridity value of six in the limiting case where outflow is zero. The conceptual figures below illustrate the impact of a positive groundwater contribution (i.e. a net flux from the surface to the subsurface) for (d) the inferred evapotranspiration and (e) direct evapotranspiration approaches.

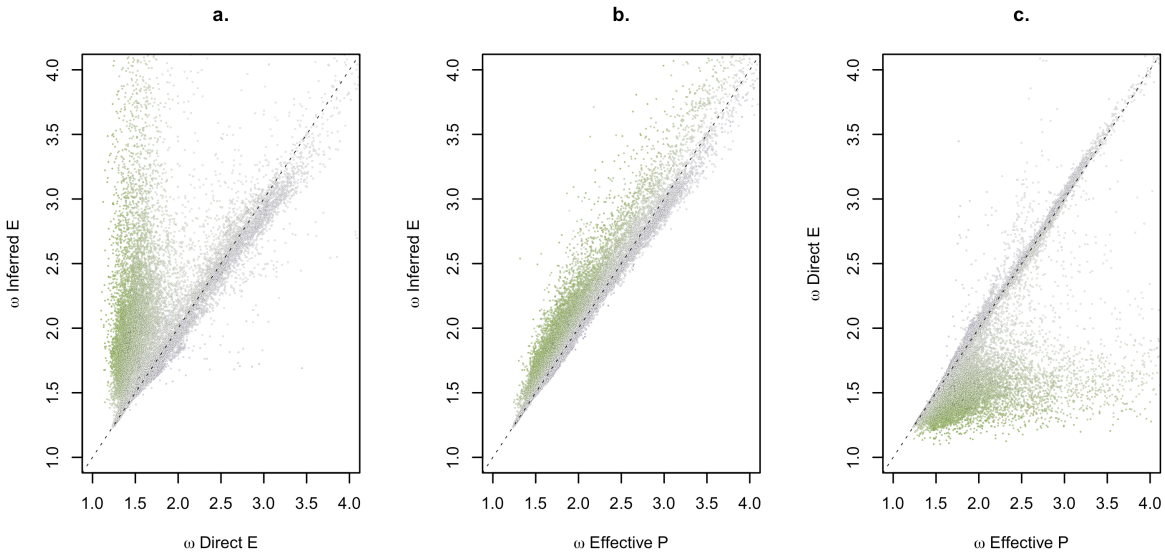

Figure 8: Comparison of shape parameters between the three approaches for every watershed. Points are colored by groundwater contribution fraction as shown in Fig. 3d. The dashed line on each plot is a one to one line for reference.

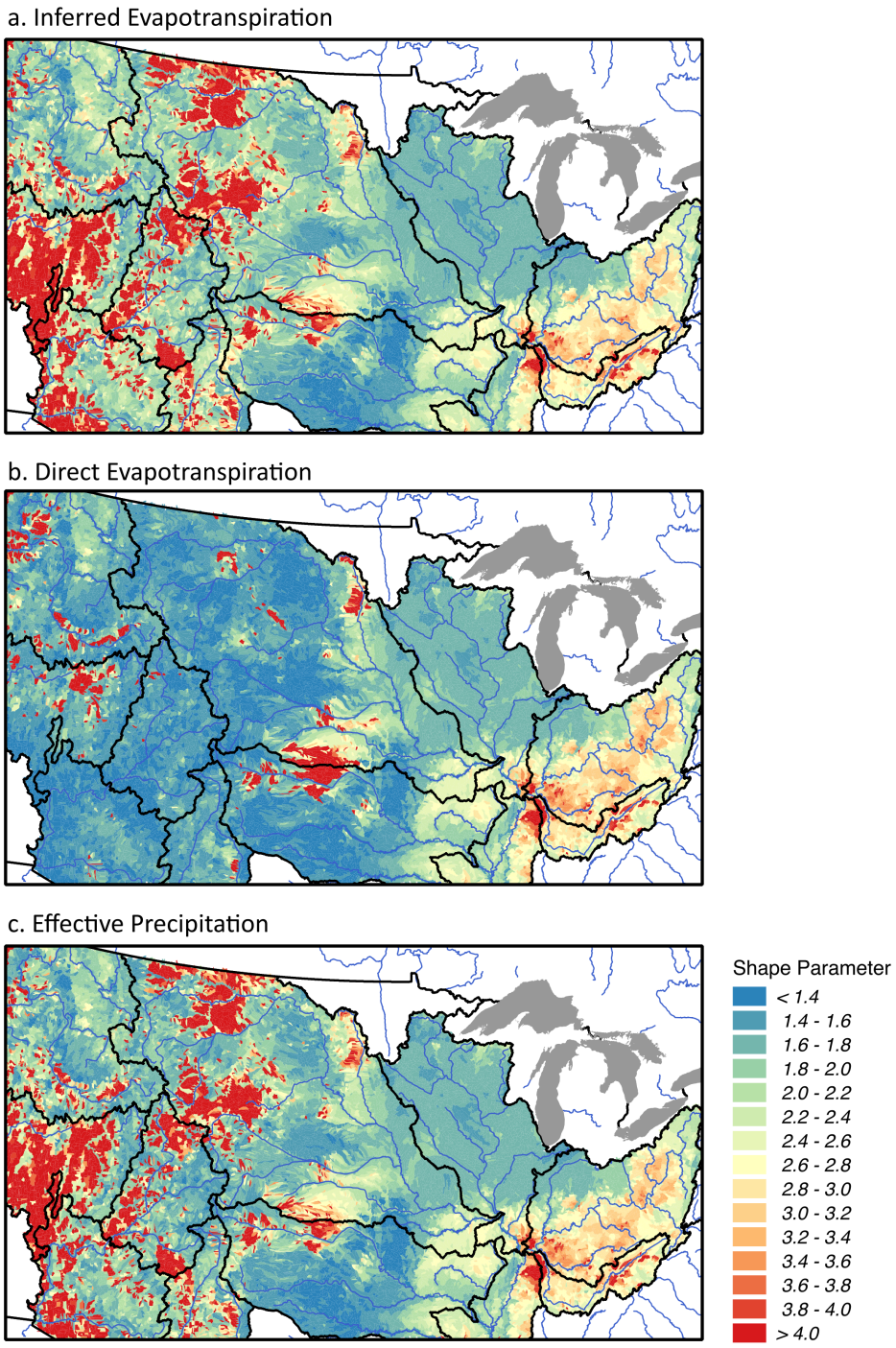

Figure 9: Map of shape parameters calculated for the 24,235 nested watersheds using the (a) inferred evapotranspiration, (b) direct evapotranspiration and (c) effective precipitation. Major rivers are outlined in blue and regional boundaries in black.

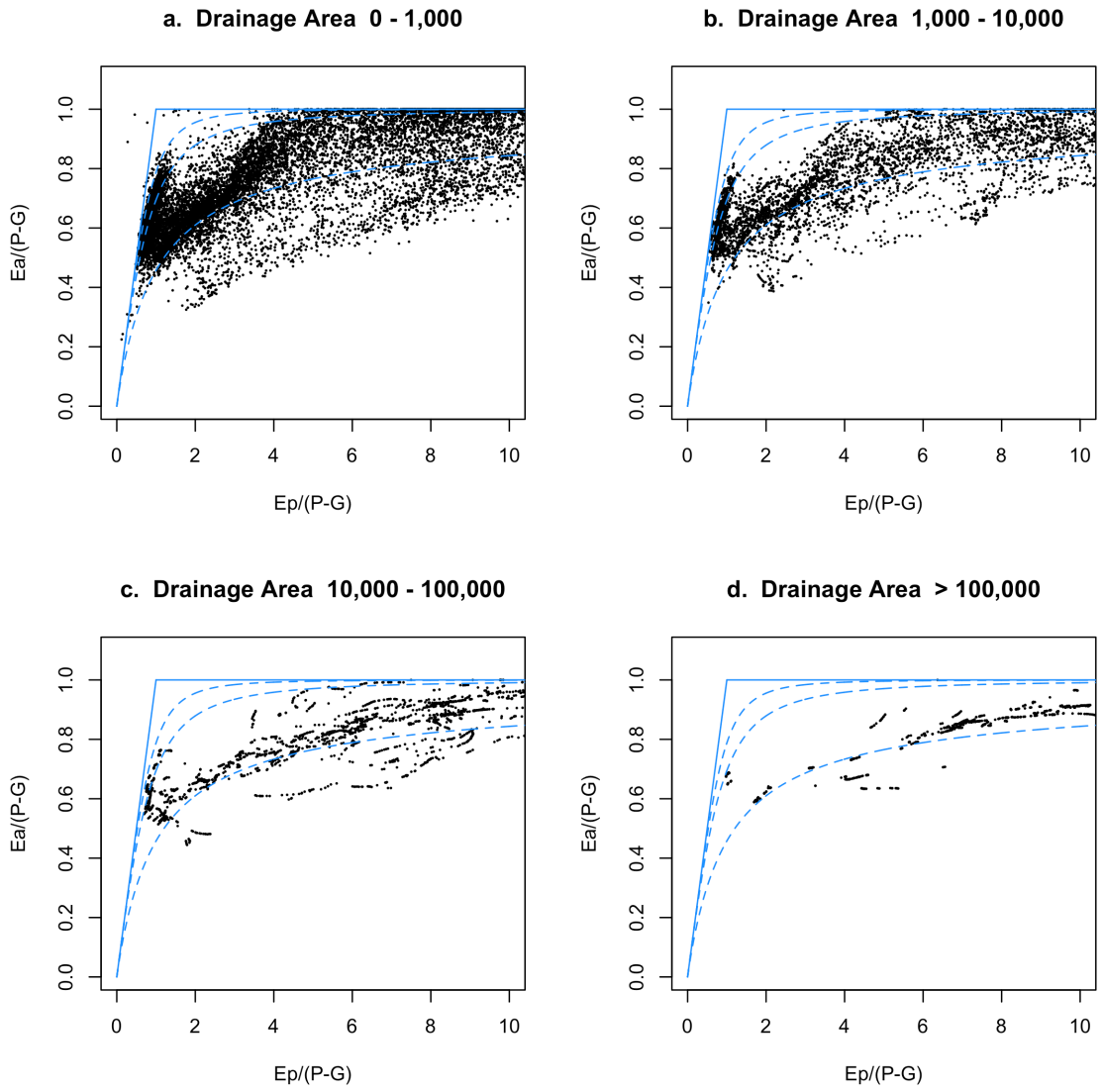

Figure 10: Budyko plots of evapotranspiration ratio versus aridity index using the effective precipitation method with watersheds grouped by drainage area [km^2]. Blue dashed lines are Budkyo curves with shape parameters of 1.6, 2.6 and 3.6 (refer to Fig. 4) and the solid blue lines show the water and energy limits.

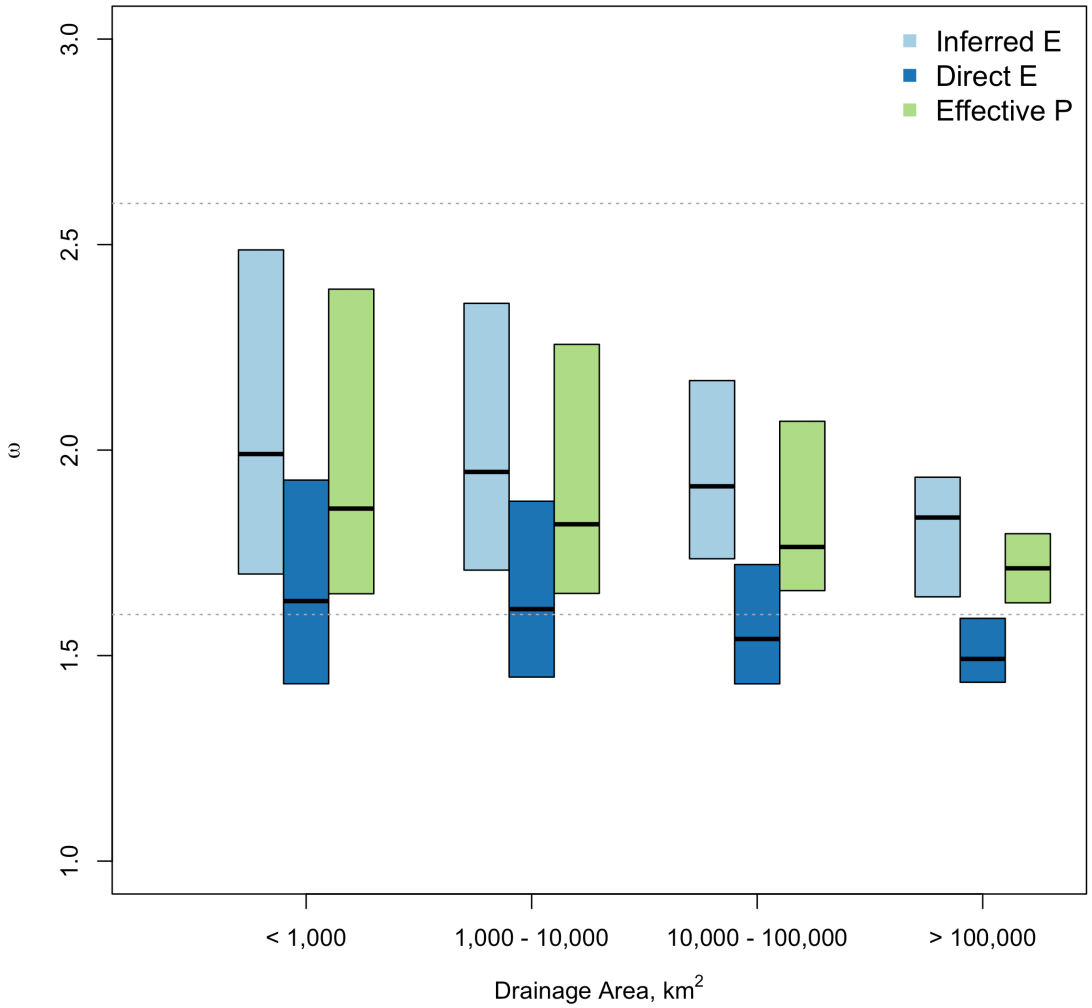

Figure 11: Boxplots showing the interquartile range (i.e. 25-75th percentile values) of shape parameters for all three approaches grouped by drainage area. Dashed lines are at 1.6 and 2.6 for reference.